



Article

A Strategy for Measuring Voltage, Current and Temperature of a Battery Using Linear Optocouplers

Gopal Reddy Lakkireddy [†] and Sudha Ellison Mathe ^{*,†}

School of Electronics Engineering, VIT-AP, University Amaravati 522237, India

* Correspondence: ellison.mathe@vitap.ac.in

† These authors contributed equally to this work.

Abstract: Input voltage, current, and temperature measurement circuits are the vital concerns of a Battery Management System (BMS) in electric vehicles. There are several approaches proposed to analyze the parameters of voltage, current, and temperature of a battery. This paper proposes a BMS methodology that is designed using linear optocouplers. In this paper, the optocouplers are incorporated between the battery pack and the BMS, which can be used in automotive applications for accurate measurements. The functions of BMS, such as measuring the current, voltage, and temperature in real time, can be executed using the proposed methodology.

Keywords: battery management system; electric vehicle; automobile; energy storage systems



Citation: Lakkireddy, G.R.; Mathe, S.E. A Strategy for Measuring Voltage, Current and Temperature of a Battery Using Linear Optocouplers. *World Electr. Veh. J.* **2022**, *13*, 225. <https://doi.org/10.3390/wevj13120225>

Academic Editors: Quanqing Yu, Yonggang Liu and Xiaopeng Tang

Received: 13 October 2022

Accepted: 17 November 2022

Published: 24 November 2022

Publisher's Note: MDPI stays neutral with regard to jurisdictional claims in published maps and institutional affiliations.



Copyright: © 2022 by the authors. Licensee MDPI, Basel, Switzerland. This article is an open access article distributed under the terms and conditions of the Creative Commons Attribution (CC BY) license (<https://creativecommons.org/licenses/by/4.0/>).

1. Introduction

Energy storage systems such as lead acid, lithium ion, nickel cadmium, sodium sulfur, zinc bromine flow battery, etc., [1] are used in electric vehicles. Among the wide range of available energy storage systems, lithium-ion batteries have high power density, high energy density, high efficiency, low discharge rate, high reliability, and a long life span [2]. Hence, lithium-ion batteries are widely used in automotive applications. The capacity and voltage of the individual battery cells used in EVs are relatively small. As a result, single battery cells must first be packed and integrated into a battery module, and the battery system in an EV frequently includes one or more modules depending on the requirements. The battery system usually consists of hundreds or thousands of single cells [3]. As a battery pack consists of several cells, BMS play an important role in:

- Protecting the cells and battery packs from being damaged;
- Making the batteries operate within the proper voltage, current, and temperature range;
- Ensuring their safety and extending their service life as much as possible;
- Maintaining the battery to operate in a state in which the batteries could fulfill the vehicle's requirements.

In electric vehicles, the safety of the battery pack is a major concern. The Battery Management System is crucial in electric vehicles, as the batteries that are being used should not get overcharged or overdischarged; it should control the cell balancing and estimate the SOC (State of Charge) and SOH (State of Health) [4–7]. These critical aspects guarantee the life of the battery by the proper measurement of the parameters and incorporating the controlling strategies accordingly so that the overcharge and overdischarge conditions can be avoided [8]. For any automotive applications or electric vehicles, it is important to measure the SOC of the cells, the current flowing in and out of the cell stack under all operating conditions, the temperature of the pack, and the individual cell voltages of each cell in the stack. The optocouplers are used to acquire the appropriate voltage values of each cell stacked in the battery pack and help us determine overall health to ensure safe operation and, along with polynomial expression, we would further be able to minimize

the error received from the optocoupler. Hence, when these two methods are amalgamated together, we achieve our idea of obtaining an error-free resolution of voltage at every cell.

2. Literature Survey

SOC ensures safe charging and discharging and is determined by considering the battery current capacity in terms of the rated capacity. The current state of the battery will be determined by the SOC and enables the batteries to safely charge and discharge [9]. The general approach for measuring SOC is to measure very accurately both the coulombs and current flowing in and out of the cell stack under all operating conditions and the individual cell voltages of each cell in the stack. The voltage method converts a reading of the battery voltage to the equivalent SOC value using the known discharge curve (voltage vs. SOC) of the battery. The need for a stable voltage range for the batteries makes the voltage method difficult to implement.

However, to measure SOC, the voltage, current, and temperature of the battery have to be measured and taken into consideration. Battery damage can be prevented by the accurate estimation of SOC, as inappropriate overcharge and overdischarge conditions can be avoided. There are different categories and methods in which SOC can be measured [5,10,11]. The categories and methods are discussed below.

2.1. Direct Measurement

Physical attributes of the batteries, such as the terminal voltage, impedance, etc., are used in direct measurement [12]. Different methods involved in direct measurement are:

2.1.1. Method of Open Circuit Voltage

The open circuit voltage is calculated by taking the SOC [13], terminal voltage, and the value of $VOC(t)$ at $SOC = 100\%$ into account. The OCV [14,15] relationship with SOC is determined by applying a pulse load on a lithium-ion battery and then allowing the battery to reach equilibrium. The OCV–SOC characteristics differ for different batteries. The problem with this method is that it is hard to figure out how the OCV and SOC are related [16].

2.1.2. Terminal Voltage Method

Terminal voltage drops are considered in this method, as there is internal impedance during the battery discharge, and hence the electromotive force of the battery is proportional to terminal voltage. This method can be employed at different temperatures and currents [17]. In this method, during discharge, the error that is estimated at the terminal voltage is greater as the battery terminal voltage drops at the end of discharge [18].

2.1.3. Impedance Method

In this method, the internal resistance of the battery is calculated by considering the battery voltage and current. The DC resistance, which is obtained from the ratio of voltage and current variation, represents the battery capacity in DC. However, the estimated value of the resistance contains an error if the time taken is longer. For the variation of SOC in a wide range, there is only a slight change in the internal resistance, which is difficult to observe [19]. For this reason, in order to estimate SOC, the DC internal resistance is rarely used [20].

2.2. Book-Keeping Estimation

The book-keeping estimation concept uses the coulomb counting method, wherein battery discharge current data are taken as input [16].

2.3. Coulomb Counting Method

In this method, the discharge current of the battery is measured and, to measure the SOC, the discharging current over time is integrated.

2.4. Adaptive Systems

The neural network, support vector machine, fuzzy neural network, and Kalman filter are the different methods that are used for estimating the SOC characteristics [16].

2.5. Hybrid Methods

The coulomb counting and EMF combination, the coulomb counting and Kalman filter combination, the per-unit system, and the EKF combination are the methods that are used in hybrid methods for analyzing SOC. Different methods are combined here to conduct the analysis [16].

The existing methodologies used for the measurement of the parameters of BMS are incorporated with the ICs. Different ICs such as ISL942002, LTC6802-2, BQ76920, MC33771, and MAX11068 [12,21–23] are used in the existing methodologies. However, using IC, we can only connect up to 12 to 14 cells. When compared with ICs, optocouplers are more beneficial regarding safe isolation, noise isolation, and galvanic isolation [13]. Optocouplers are used to monitor the system voltage and the voltage across each cell of the battery pack, including the determination of overall health to ensure safe operation. Depending on the configuration and number of cells in the battery pack, different architectures are available. With the use of optocouplers, we can connect an arbitrary number of cells. As we are using optocouplers, there is not direct contact between the battery and the BMS unit. As a result, we can precisely measure the voltage of each and every series cell.

2.6. VOMA618A

The VOMA618A optocoupler is used to monitor the battery voltage with safe isolation (galvanic isolation), as there is not any direct contact between the primary and secondary circuits [13]. The peak forward current in this optocoupler is 0.5 Amp. However, the optocoupler used in the proposed system has 1 Amp, and hence the circuit is more resistant to short-circuit current. The reverse voltage protection in the VOMA618A is up to 5 V, but in the proposed methodology, the optocoupler has a high reverse voltage protection that is up to 6 V.

2.7. IL300

IL300 is a linear galvanic isolation optocoupler, where the feedback photocoupler captures the LED's flux percentage and generates a control signal that is used to servo the drive current of the LED [11,13]. This optocoupler has a reverse voltage of 5 V, whereas the optocoupler used in the proposed methodology has a reverse voltage of 6 V. This optocoupler has a power dissipation of 160 mW, whereas the optocoupler used in the proposed methodology has a power dissipation of 70 mW.

As conventional lithium-ion batteries are based on the intercalation mechanism, charging at high capacity should be considered wisely. Lithium nickel manganese cobalt oxide (NMC) makes the future scope [24]. When used for energy storage systems, li-ion batteries' material chemistry plays a role in the long-time cell performance and storage capacity of the cell. So, the charging and discharging of the cell need to be taken so the temperature of the cell does not rise due to electrochemical reactions in electrolytes [25]. The performance and longevity of any fuel cell are based on the chemical composition and inflow condition of that cell, which is based on catalytic partial oxidation [26].

This research is focused on the usage of optocouplers to measure each cell's voltage. A current sensor is used to measure the current of the total pack. An NTC thermistor is used to measure the temperature of the total pack. The paper is mainly focused on the measurement of the voltage of each cell, total charge current, the temperature of the entire pack, and charge and discharge state. The benefit of the proposed system can be elucidated as we are using an optocoupler with an ESP32 microcontroller. The ESP32 microcontroller has a 12-bit ADC (Analog to Digital Converter), and hence the resolution of the voltage is higher. In turn, the voltage can be measured more accurately in microvolts. We used an optocoupler to reduce the difficulty in measuring the voltage of the cells that are connected

in series. Based on the integration of linear optocouplers with galvanic isolation for BMS, a method was proposed to measure voltage. This method has a sensitivity of 0.003 V [13].

In the proposed methodology, as we used an optocoupler with a 12-bit ADC, we obtained a resolution of 0.00081 V. The optocoupler is supplied with a voltage of 2.7 V to 4.2 V on the primary side, and the voltage range on the secondary side varies from 0 V to 3.33 V. The nominal voltage of most lithium-ion cells is 3.7 V per cell, the minimum cut-off is about 2.7 V, and the maximum is 4.2 V, respectively. The minimum voltage, maximum voltage, and operating voltage of the microcontroller are 2.7 V, 4.2 V, and 3.33 V, respectively. The theoretical calculation for the obtained resolution using the proposed topology is calculated by the following expression:

$$Resolution = \frac{V_{max}}{adc_{resolution}} \quad (1)$$

$$Resolution = \frac{3.3}{4096} = 0.00081 \text{ V} \quad (2)$$

where V_{max} = Microcontroller Operating Voltage = 3.3 V and $adc_{resolution}$ = 4096 Bits.

3. Proposed Methodology

The number of modules and the batteries that are connected depend on the architecture of the battery pack and the maximum voltage that is required. In this design, we consider 16 cells to form a battery pack. Figure 1 represents a single module in which two cells are connected in parallel. Figure 2 depicts eight modules connected in series, with each module consisting of two cells in parallel. Across each module, an optocoupler is connected. The output of the optocoupler is given to the ESP32 microcontroller. An NTC (thermal sensor), a WCS1800, a display unit, two transistors, and two MOSFETs are connected to the microcontroller. The battery that is used in the design is a li-ion NMC (lithium-ion nickel manganese cobalt) battery with 3.7 V and 2500 mAh. Figure 3 helps us understand the measurement of voltage, current and temperature of a battery pack connected with the microcontroller using linear optocoupler.

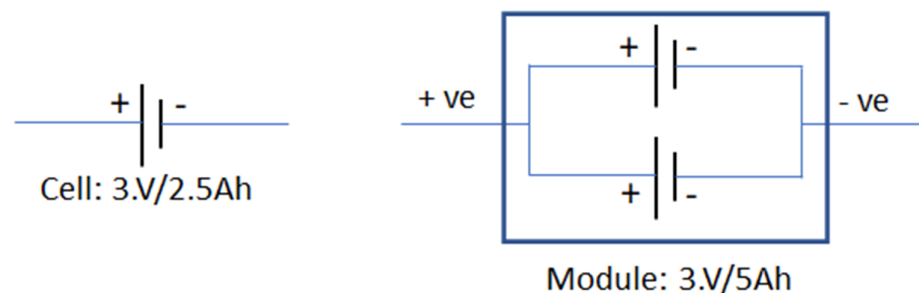


Figure 1. Cell and module configuration.

3.1. Voltage Measurement

An optocoupler is connected across each cell, wherein the cell voltage is given as the input to the voltage measurement circuit. The LED in the optocoupler glows according to the voltage that is impressed on the circuit. When the LED glows, the resistance of the photodiode decreases accordingly. If the glowing intensity of the LED decreases further, the resistance increases. The voltage sample at the collector terminal is given to the microcontroller. The output of the microcontroller is connected to two MOSFETs, which are connected in series with respect to their negative terminals. These MOSFETs turn on and off under the conditions of overcharge and overdischarge. The voltage measurement circuit is shown in Figure 4.

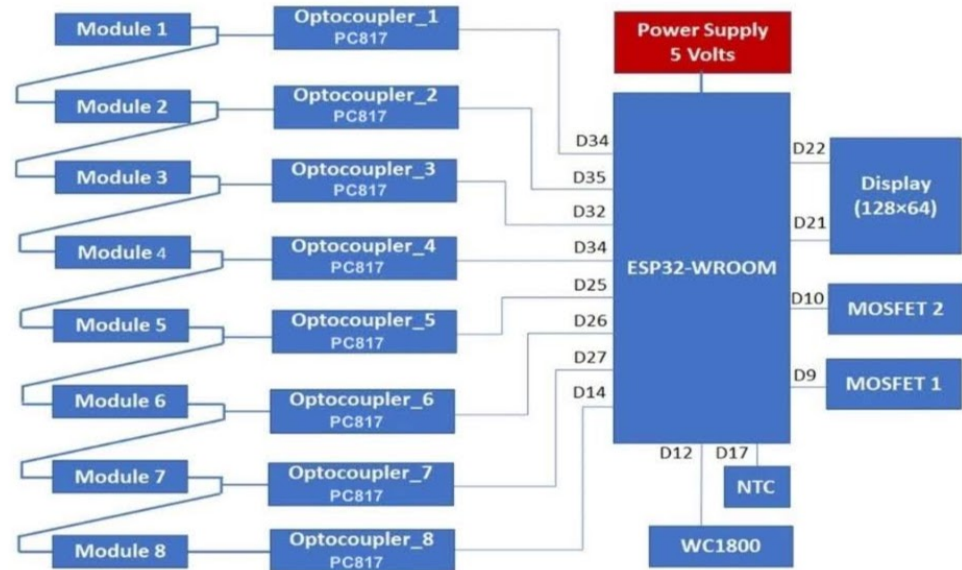


Figure 2. Block diagram of the proposed methodology.

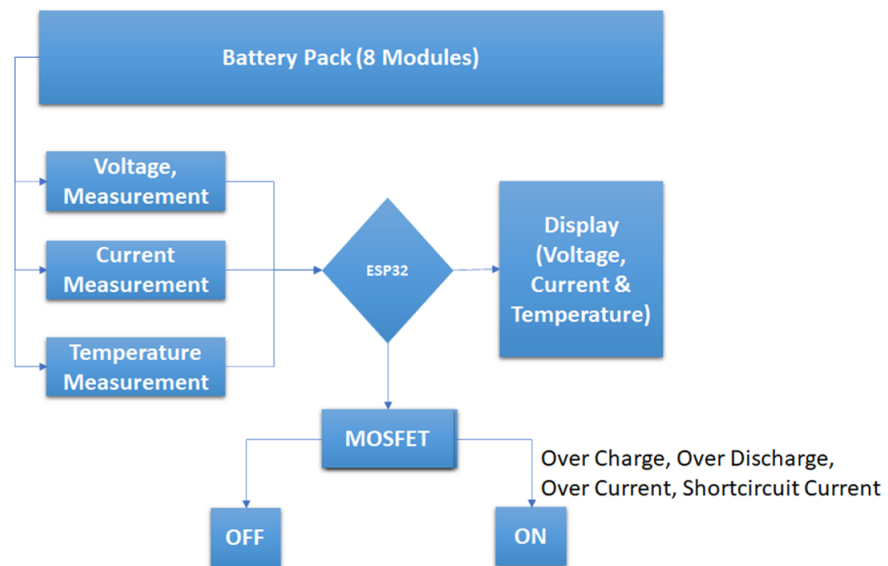


Figure 3. Flow chart for measuring voltage, current, and temperature of a battery using linear optocouplers.

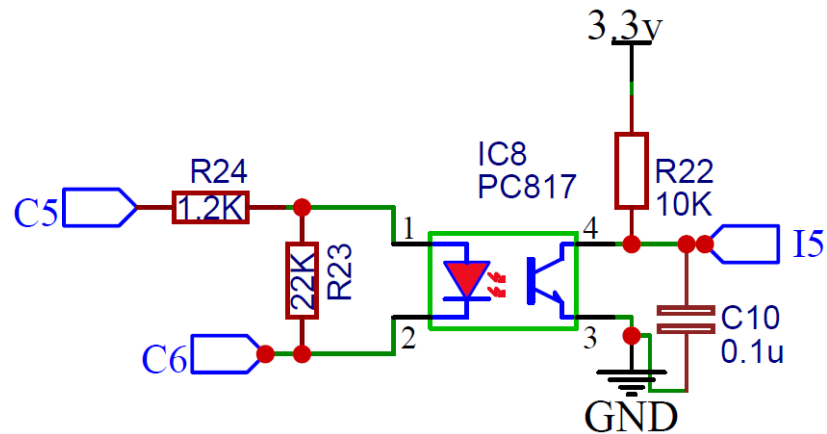


Figure 4. Voltage measurement circuit.

C1 and C2 are the positive and negative terminals of Cell-1. The resistors R33 and R34 act as voltage dividers. An optocoupler with 4 terminals is connected to an LED on the primary side and a photocoupler on the secondary side. The reference voltage is 3.3 V, which is connected to a pull-up resistor R35 and is coupled to the collector terminal of the photodiode. The emitter terminal of the photodiode is grounded. The circuit is analyzed under the following conditions:

- When the LED does not glow: Under this condition, the voltage at the collector terminal is equal to the reference voltage, as there is not a change in the resistance of the photodiode.
- When the LED glows: Under this condition, the resistance of the photodiode changes. Due to this change in the resistance, the voltage at the collector terminal is changed. The change in the voltage depends upon the parameters of the intensity of the LED glow and the resistance of the photodiode.

If the intensity of the LED glow is 20%, the resistance of the photodiode decreases when compared with its actual resistance, which in turn lets the voltage flow through the emitter terminal. The resultant voltage with respect to the reference voltage and the emitter voltage appears across the collector terminal. This voltage sample that appears across the collector terminal is given to the microcontroller, and depending on the voltage at the collector terminal, the battery voltage is determined. If the brightness of the LED light goes from 20% to 40%, the photodiode's resistance goes down even more, which changes the voltage at the collector terminal. We cannot determine the actual voltage by knowing the linear values because of this nonlinear functionality. So, with the resolution of 0.05 V steps, we took the ADC values and then put them on the microcontroller by applying the linear interpolation formula to those values. The input voltage, ADC value, and the difference are mentioned in Table 1.

Table 1. Sample Values of the Proposed Topology.

Input Voltage of Optocoupler (Volts)	<i>adc_{value}</i>	Difference
2.05	4100	61
2.1	4039	59
2.15	3980	54
2.2	3926	51
2.25	3875	61
2.3	3814	66
2.35	3748	57
2.4	3691	66
2.45	3625	66
2.5	3559	... Continue

Linear interpolation is a way to fit a curve that uses polynomials to make new data points within the range of a set of discrete data points that are already known. Linear interpolation is a polynomial method that helps us find the missing values of the voltage in the battery pack and, after taking a sample, the polynomial expression is used to obtain the accuracy and further minimize the error in obtaining the voltage measurement.

The linear interpolation method is used after taking a sample of the polynomial expression to obtain the accuracy of voltage measurement. Here, the purpose to use this method is to even out the desired difference in the ADC value. As the resolution is varied with 0.05 V, we received a specific ADC value for every change in the primary side, but the difference of the ADC value is not in constant proposition with an increase in the input voltage of the optocoupler, and that is why this method helps us minimize the error occurring with the proposed methodology of using an optocoupler. This method is applied to the sampled values of the ADC in the microcontroller.

$$y = y_1 + (x - x_1) \frac{y_2 - y_1}{x_2 - x_1} \quad (3)$$

Here, y_1 is the voltage of the battery we want to know (linear interpolation value), x_1 is the ADC value at y (independent variable), x_1 and x_2 are the values in between x that can be calculated, and y_1, y_2 is the input voltage of the optocoupler which we want to calculate. This linear interpolation method is incorporated into the microcontroller using the above-given Formula (3), and the acquired results then showcase in the experimental setup.

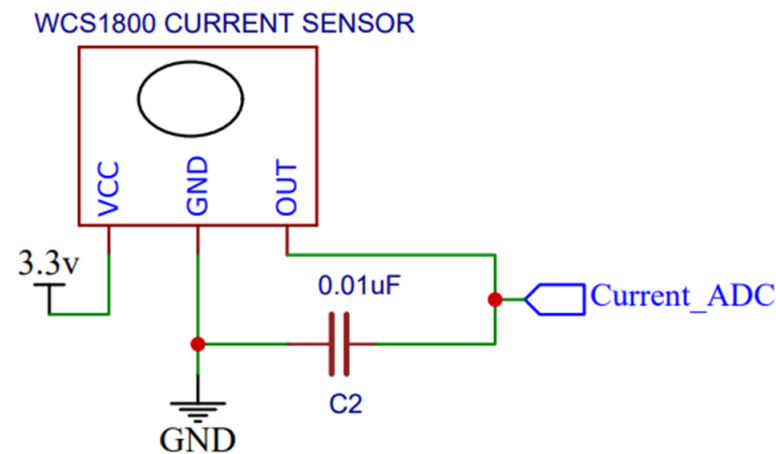


Figure 5. Current measurement circuit.

3.2. Current Measurement

A sensor, WCS1800, is incorporated into the system to measure the current of the total pack. The terminal of the sensor is connected to the microcontroller. The measured current is measured by the MOSFET that is connected to the output terminal of the microcontroller, and accordingly, the MOSFET turns off during the conditions of overcurrent and short-circuit current. The current measurement circuit is shown in Figure 5. The ADC value is calculated by (4)

$$x = \frac{x_S}{x_R} \times V_{op} - V_{er} \quad (4)$$

where $x = adc_{value}$, $x_S = \text{Sensor output value}$, and $x_R = adc_{resolution}$
Current can be calculated by the expression (iv)

$$current = x \times sensitivity \quad (5)$$

where $adc_{resolution} = 12 - \text{bit} = (2)^{12} = 4096$ bits, operating voltage = 3.3 V, sensitivity of current sensor = 475.42, and error voltage = 1.65 V.

3.3. Temperature Measurement

An NTC glass thermistor is connected to pin 13 of the microcontroller to measure the temperature of the total pack. The temperature measurement circuit is shown in Figure 6. When supply voltage is given to the temperature measurement circuit, if the temperature is 0, resistance R31 is high. The value of resistance R31 varies depending upon the variation in temperature. If the resistance R31 decreases, then the voltage flow in the circuit increases, which results in an increase in the temperature. The temperature that is being varied is sensed accordingly.

Temperature measurement circuit parameters:

```
Const double A = 0.001129148;
Const double B = 0.000234125;
Const double C = 0.0000000876741;
Const double VCC = 3.3 // Esp32 on board 3.3 V VCC;
Const double R32 = 10,000 // 10 k ohm series resistor;
Const double adcResolution = 4096;
adcValue(Tempadc) = analogRead(12).
```

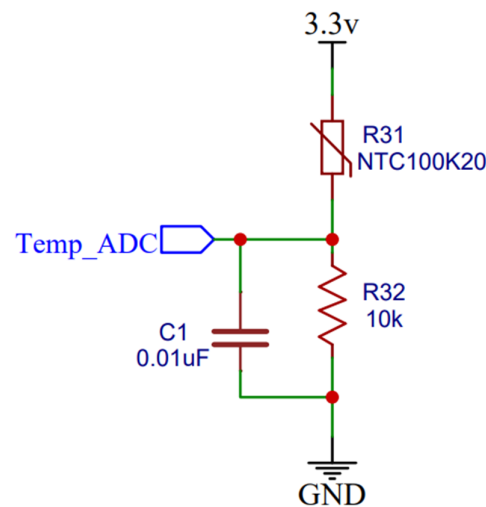


Figure 6. Temperature measurement circuit.

Measurement of Temperature

$$V_{out} = \frac{adc_{value} \times V_{CC}}{adc_{resolution}} \quad (6)$$

$$R_{th} = \frac{V_{CC} \times R_{32}}{V_{out}} - R_2 \quad (7)$$

As per the equation of Steinhart–Hart thermistor:

$$TemperatureinKelvin = \frac{1}{\{A + B[\ln(R)] + C[\ln(R)]^3\}} \quad (8)$$

where $A = 0.001129148$, $B = 0.000234125$, $C = 8.76741 \times 10^{-8}$, and $temperature = temperature - 219.15$

Display Unit:

A display unit is used to exhibit the state of charge and discharge condition. The voltage of cells, temperature, and current of battery packs are shown in the display unit.

Optocoupler:

The optocoupler that is used in the design consists of an IR LED (Infrared Light-Emitting Diode) on the primary side and a phototransistor on the secondary side. The resistance of the phototransistor changes according with the intensity of the LED's brightness. Then, accordingly, the collector terminal voltage varies. The PC817 optocoupler has a high reverse voltage protection that is up to 6 V compared with VOMA618A and IL300 and has a power dissipation of 70 mW. It features a high current transfer ratio at low input current, low coupling capacitance, and high isolation voltage. It helps design electronic circuits where there is a possibility for voltage surge or voltage spikes which may damage the circuit components. It is also used to eliminate noise from the signal and segregate DC circuits with low voltage from AC circuits with high voltage. The optocouplers monitor the system voltage and the voltage across each cell and are also used to eliminate noise from the signal. They feature a high current transfer ratio at low input current, low coupling capacitance, and high isolation voltage. This coupling device is designed for signal transmission between two electrically separated circuits, specifically for use in automotive as well as highly reliable industrial applications.

Microcontroller:

An ESP32 microcontroller is used in the design. The voltage variation at the collector terminal is given as an input to the microcontroller GPIO pin. The battery voltage is determined according to the voltage that is being varied at the collector terminal of the

optocoupler. The major purpose of using this particular microcontroller is because of the low sampling rate of the values at 132 ms.

Transistor:

We used BC547 as a transistor, which is usually used for current amplifiers, quick switching, and pulse-width modulation (PWM). Therefore, if you need to control the speed of the actuator, using this transistor can achieve it. BC547 is mainly used for amplification and switching purposes. The transistor seems to have a better cutoff frequency and a high current gain.

MOSFET:

An IRFZ44 MOSFET is used, which acts as a switch. The MOSFET operates under the conditions of high current, high voltage, undercurrent, and undervoltage. The overcharge and overdischarge control circuit is shown in Figure 7. Two MOSTETs, T1 and T2, are connected in series along with transistors Q1 and Q2 to the terminals of the microcontroller. A transistor is connected across each MOSFET to turn on and off the MOSFET under the conditions of overdischarge and underdischarge. During the conditions of overdischarge and underdischarge, the circuit acts as an open circuit.

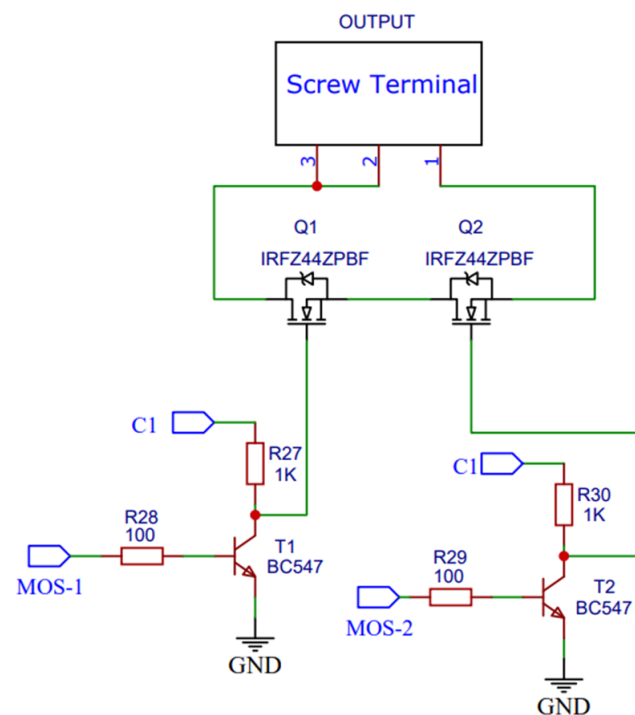


Figure 7. Overcharge and overdischarge control circuit.

Ideal Condition:

In the ideal condition, charging and discharging of the battery is possible. Q1 and Q2 are on. Diodes D1 and D2 are on, as shown in Figure 8.

1. Charging

During charging, the current flows from the charger to the battery through D2 and Q1. During this process, Q2 is off, and D1 is reverse-biased.

2. Discharging

During discharging, the current flows from the battery to the charger through Q2 and D1. During this process, Q1 is off, and D2 is reverse-biased.

3. Over charge

If overcharge is detected, Q1 goes off, and the charge does not flow from charger to the battery. During this condition, Q1 is off, Q2 is on, and D2 is on. The current flows from the charger to the battery through the freewheeling diode D2 and Q1. The overdischarge condition is shown in Figure 9.

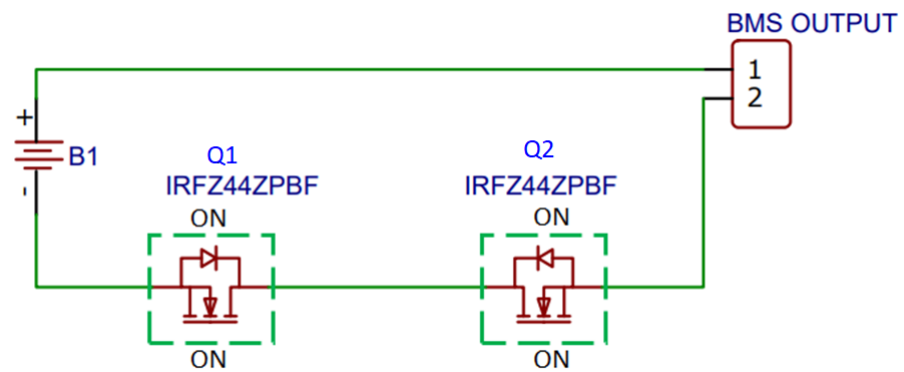


Figure 8. MOSFET in ideal condition.

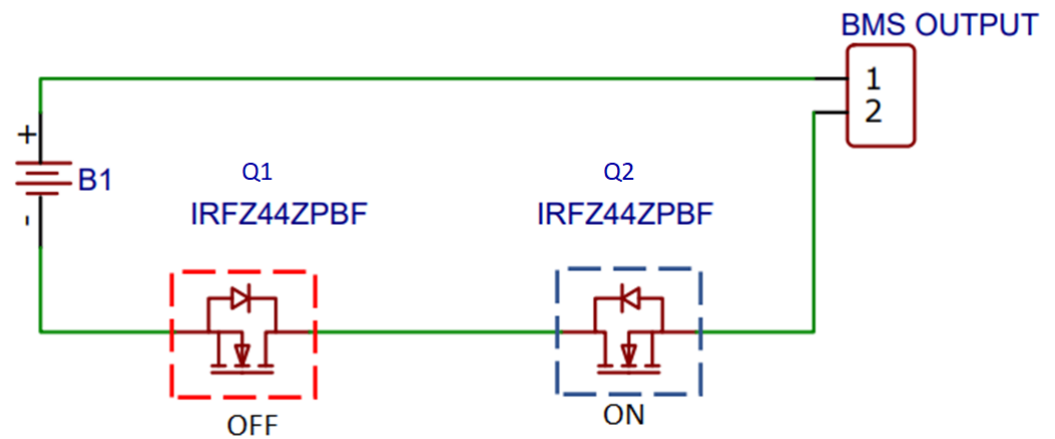


Figure 9. MOSFET in overcharge condition.

4. Overdischarge

When overdischarge is detected, Q2 is off, and the charge does not flow from battery to the load. During this condition, Q1 is on, D1 is on, and Q2 is off. The current flows from battery to the load through Q2 and D1. The overdischarge condition is shown in Figure 10.

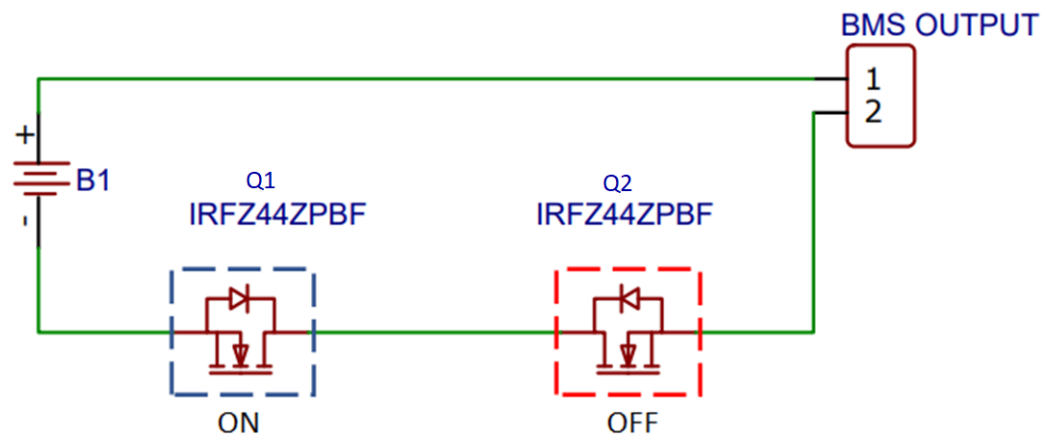


Figure 10. MOSFET in overdischarge condition.

4. Experimental Setup

The experimental setup shown in Figure 11 was built and experimented on. All the design elements that are incorporated in the experiment as shown in the experimental setup were already mentioned and described in Section 3 of the proposed methodology.

In the initial condition, the battery pack is charged fully to 32.61 V. The IC load is connected to the battery pack. The load consumes a current of 5 amps. The battery completely discharges to 25.52 V in a period of 1 h. A 1 C or 1000 mA rate means this

particular discharge current will fully discharge the battery in 1 h; likewise, a standard charge on a datasheet was defined as 0.5 C or 500 mA, i.e., the charge current is half the battery capacity, which means it takes over 2 h to fully charge. During the instance of Cell 3 being discharged to 2.6 V, an undervoltage condition is detected, the MOSFET turns on, and the loads disconnect. During the instance of Cell 1 being charged to a voltage of 4.2 V, the overcharge condition is detected and the MOSFET turns on, and the charging process stops. The corresponding values of each cell and total pack are mentioned in Table 2 with respect to the plots in Figures 12 and 13.

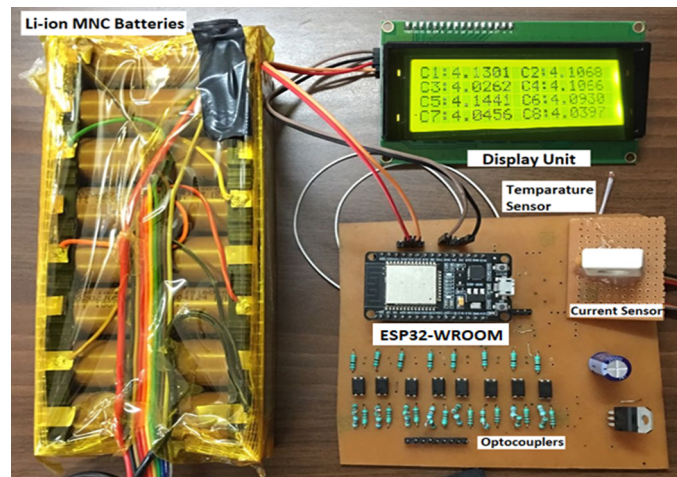


Figure 11. Experimental setup.

Table 2. Individual Cell Voltages with Respect to Charge and Discharge State.

Charge/Discharge	Starting/Cut-Off	Cell 1	Cell 2	Cell 3	Cell 4	Cell 5	Cell 6	Cell 7	Cell 8	Total
Discharging	Starting	4.130769	4.068254	4.005384	4.06666	4.06111	4.10919	4.10298	4.06951	32.61387
	Cutoff	3.339344	3.244366	2.670313	3.30454	3.23333	3.27641	3.3022	3.20375	25.55226
Charging	Starting	3.584058	3.577273	3.534746	3.55808	3.56102	3.53292	3.51818	3.52777	28.39408
	Cutoff	4.204268	4.1875	4.109524	4.16095	4.17443	4.15393	4.11044	4.11214	33.2132

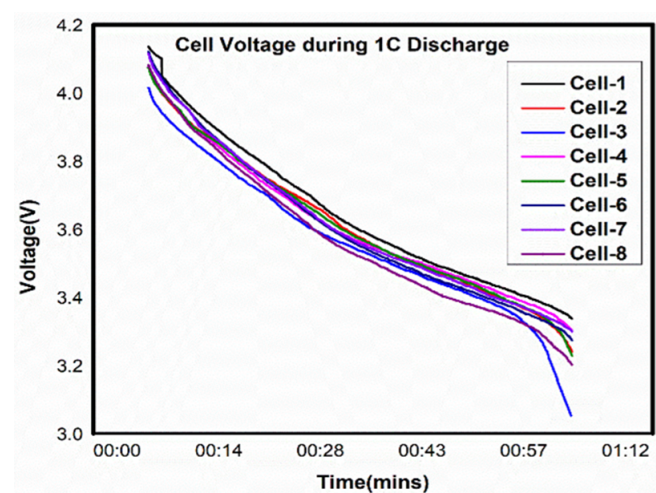


Figure 12. Discharge curve plot for individual cells.

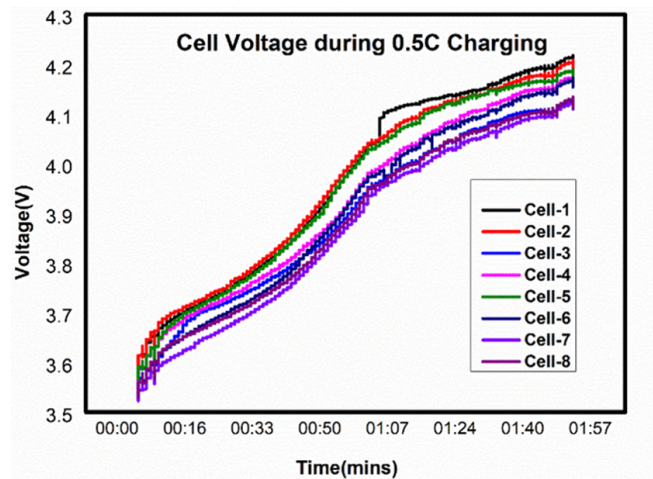


Figure 13. Charge curve plot for individual cells.

The battery is charged with 0.5 C with starting and cutoff voltages range from 28.39 V to 33.4 V. The charging and discharging curves that are obtained are represented in the below Figures 14 and 15, respectively. During discharge, the starting and cutoff voltages ranges from 32.61 V to 25.22 V.

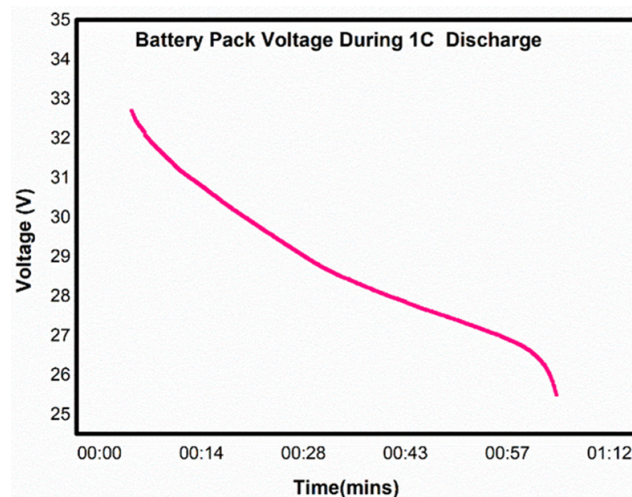


Figure 14. Discharging curve.

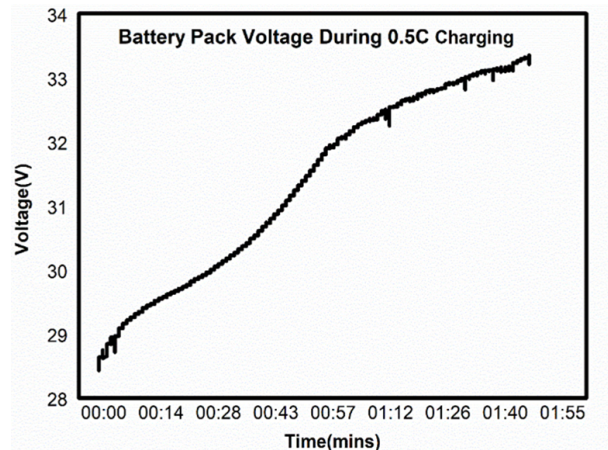


Figure 15. Charging curve.

Table 3. Experimental Results.

Input Voltage (V_b Cell)	ADC Values	Output Voltage (V_{out})	V_b Cell – V_{out} (mV)	Relative Error (%)
2.1	4039	2.101	1	0.04759638
3	2962	3.003	3	0.10987913
3.5	2385	3.502	2	0.0456934
3.8	2005	3.803	3	0.07362996
4	1744	4.004	4	0.10239505
4.2	1472	4.205	5	0.12365643

The respective values of each cell and the total pack are mentioned in the table with respect to the graph in Figure 13. The charge and discharge plots are projected in Figures 12 and 13, respectively. The above Figure 13 helps us understand the charge curve of individual cells in a battery module. Here, the plot shows the voltage and charging time, when each cell has been charged and reached its full charge voltage at a coulomb rate of 0.5 C, with a charging time of 2 h. The above Figure 12, helps us understand the discharge curve of individual cells in a battery pack with parameters such as voltage and discharging time when each cell has discharged and reached its full discharge voltage at a coulomb rate of 1 C in one hour.

The measurement was first taken by the standard multimeter named Fluke 115 for measuring the voltage and current parameters. So, the comparative measurement between the multimeter and our proposed methodology is shown below in Table 3.

The following equation is used to calculate error from the experimental data:

$$e_r = \frac{V_{out} - V_b}{V_b} \times 100 \quad (9)$$

Here e_r = relative error; V_{out} = output voltage; and V_b = battery input voltage.

Here, the input voltage (V_b cell) is the voltage taken at the primary side of the optocoupler, which was measured using a Fluke multimeter. For every 0.5 V variation in input voltage, we obtain certain ADC values, i.e., at the secondary side of the optocoupler, which is connected to the microcontroller. After the microcontroller receives the ADC values, we sampled those ADC values and applied the linear interpolation method, and the resultant output we received at the output end of the microcontroller is V_{out} (output voltage). So, after applying the error calculation formula, we can conclude the relative error difference received before and after using the optocoupler and linear interpolations method. The experimental results show the maximum error is 0.123656425 and minimum error is 0.045693397.

5. Conclusions

Real-time analysis of BMS is carried out with the proposed topology for measuring each cell voltage, total pack current, and total pack temperature with more accuracy, along with the investigation of charge and discharge conditions. In the method of measuring the voltage with the use of linear optocouplers with galvanic isolation, the sensitivity observed is 0.003 V. In the proposed methodology, wherein an optocoupler was used with a 12-bit ADC, the resolution was observed to be 0.00081 V. As a result of the real-time analysis, the maximum error present in the proposed system is 0.123 and in existing topologies is 0.384. The measurement of crucial parameters of BMS, such as voltage, current, and temperature, is measured, and more accurately measured, when compared with the existing topologies. The proposed use of optocouplers helps us acquire the appropriate voltage values of every cell stacked in the battery pack and helps us determine overall health to ensure safe operation. Along with the polynomial expression, we would further be able to minimize the error received from the optocoupler. Optocouplers monitor the system voltage and the voltage across each cell, including the determination of overall health to ensure safe operation. By using optocouplers, there is no direct contact between the battery and the BMS unit. As a result, we can precisely measure the voltage of every series cell more accurately with nearly negligible error without disturbing the battery or the BMS.

Hence, when these two methods are amalgamated, we achieve our idea of obtaining an error-free resolution of voltage at every cell.

Author Contributions: Conceptualization, methodology, software, data curation, investigation, writing—original draft preparation: G.R.L.; Validation, formal and deep analysis, resources, writing review and editing, supervision, project administration: S.E.M. All authors have read and agreed to the published version of the manuscript.

Funding: The authors received no financial support for the research, authorship, and/or publication of the article.

Data Availability Statement: Not applicable.

Conflicts of Interest: The authors declare that there are no conflict of interest.

References

1. Brandi, M.; Gall, H.; Wenger, M.; Lorentz, V.; Giegerich, M.; Baronti, F.; Fantechi, G.; Fanucci, L.; Roncella, R.; Saletti, R.; et al. Batteries and battery management systems for electric vehicles. In Proceedings of the IEEE Design, Automation Test in Europe Conference Exhibition, Dresden, Germany, 12–16 March 2012.
2. Miao, Y. Current Li-Ion Battery Technologies in Electric Vehicles and Opportunities for Advancements. *Energies* **2019**, *12*, 1074. [[CrossRef](#)]
3. Cherukuri, M.; Kanthi, M. Battery Management System Design for Electric Vehicle. In Proceedings of the IEEE International Conference on Distributed Computing, VLSI Electrical Circuits and Robotics, Manipal, India, 11–12 August 2019.
4. Yup, T.; Wu, L.; Zhang, X.; Tian, G. High-precision voltage measurement IP core for battery management SoC of electric vehicles. In Proceedings of the IEEE International Conference on Solid-State and Integrated Circuit Technology, Guilin, China, 28–31 October 2014; pp. 1–3.
5. Mawonou, K.S.R.; Eddahech, A.; Dumur, D.; Godoy, E.; Beauvois, D.; Mensler, M. Li-Ion Battery Pack SoC Estimation for Electric Vehicles. In Proceedings of the 44th Annual Conference of the IEEE Industrial Electronics Society, Washington, DC, USA, 21–23 October 2018; pp. 4968–4973.
6. Xiong, R.; Li, L.; Tian, J. Towards a smarter battery management system: A critical review on battery state of health monitoring methods. *J. Pow. Sour.* **2018**, *405*, 18–29. [[CrossRef](#)]
7. Shah, F. A.; Sheikh, S.S.; Mir, U.I.; Athar, S.O. Battery Health Monitoring for Commercialised Electric Vehicle Batteries: Lithium-Ion. In Proceedings of the International Conference on Power Generation Systems and Renewable Energy Technologies, Istanbul, Turkey, 26–27 August 2019; pp. 1–6.
8. Buccolini, L.; Ricci, A.; Scavongelli, C.; DeMaso-Gentile, G.; Orcioni, S.; Conti, M. Battery Management System (BMS) simulation environment for electric vehicles. In Proceedings of the IEEE 16th International Conference on Environment and Electrical Engineering, Florence, Italy, 7–10 June 2016; pp. 1–6.
9. Cheng, K.W.E.; Divakar, B.P.; Wu, H.; Ding, K.; Ho, H.F. Battery-Management System (BMS) and SOC Development for Electrical Vehicles. *IEEE Trans. Veh. Technol.* **2011**, *60*, 76–88. [[CrossRef](#)]
10. Vaideeswaran, V.; Bhuvanesh, S.; Devasena, M. Battery Management Systems for Electric Vehicles using Lithium-Ion Batteries. In Proceedings of the IEEE Innovations in Power and Advanced Computing Technologies (i-PACT), Vellore, India, 22–23 March 2019; pp. 1–9.
11. Dimitrov, B.; Collier, G.; Cruden, A. Design and Experimental Verification of Voltage Measurement Circuits Based on Linear Optocouplers with Galvanic Isolation for Battery Management Systems. *World Electr. Veh. J.* **2019**, *10*, 59. [[CrossRef](#)]
12. Danko, M.; Adamec, J.; Taraba, M.; Drgona, P. Overview of batteries State of Charge estimation methods. *Transp. Res. Proc.* **2019**, *40*, 186–192. [[CrossRef](#)]
13. Wang, H.; Liu, Y. Estimation of state of charge of batteries for electric vehicles. *Int. J. Control Autom.* **2013**, *6*, 185–194.
14. Chang, W.Y. The state of Charge Estimating Methods for Battery: A review. *Int. Sch. Res. Not.* **2013**, *2013*, 953792. [[CrossRef](#)]
15. Anbuky, A.H.; Pascoe, P.E. VRLA battery state-of-charge estimation in telecommunication power systems. *IEEE Trans. Ind. Elec.* **2000**, *47*, 565–573. [[CrossRef](#)]
16. Wang, Y.; Tian, J.; Sun, Z.; Wang, L.; Xu, R.; Li, M.; Chen, Z. A comprehensive review of battery modeling and state estimation approaches for advanced battery management systems. *Renew. Sustain. Energy Rev.* **2020**, *131*, 110015. [[CrossRef](#)]
17. Lu, L.; Han, X.; Jianqui, L.; Hua, J.; Ouyang, M. A review on the key issues for lithium-ion battery management in electric vehicles. *J. Pow. Sour.* **2013**, *226*, 272–288. [[CrossRef](#)]
18. Hannan, M.A.; Lipu, M.S.H.; Hussain, A.; Mohamed, A. A review of lithium-ion battery state of charge estimation and management. *Renew. Sustain. Energy Rev.* **2017**, *78*, 834–854. [[CrossRef](#)]
19. Liu, P.; Zhang, X. The Design of Smart Battery Management Systems. *J. Comput.* **2011**, *6*, 2484–2490. [[CrossRef](#)]
20. Vitols, K. Design of an Embedded Battery Management System with Passive Balancing. In Proceedings of the 6th European Embedded Design in Education and Research IEEE, Milan, Italy, 11–12 September 2014.

21. Pitorac, C. An Inside Look in The Electrical Structure of the Battery Management System Topic Number: Renewable Power Sources, Power Systems and Energy Conversion. *Int. J. Technol. Res. Appl.* **2015**, *3*, 8–12.
22. Martins, D.; Kruck, A.M. Optocouplers in On-Board Chargers and Battery Monitoring Systems. 2019. Available online: <https://www.vishay.com/docs/80224/applicationnote92.pdf> (accessed on 13 October 2022).
23. Zhou, W.; Zheng, Y.; Pan, Z.; Lu, Q. Review on the Battery Model and SOC Estimation Method. *Processes* **2021**, *9*, 1685. [CrossRef]
24. Divakaran, A.M.; Minakshi, M.; Bahri, P.A.; Paul, S.; Kumari, P.; Divakaran, A.M.; Manjunatha, K.N. Rational design on materials for developing next generation lithium-ion secondary battery. *Prog. Solid State Chem.* **2021**, *62*, 100298. [CrossRef]
25. Divakaran, A.M.; Hamilton, D.; Manjunatha, K.N.; Minakshi, M. Design, Development and Thermal Analysis of Reusable Li-Ion Battery Module for Future Mobile and Station-ary Applications. *Energies* **2020**, *13*, 1477. [CrossRef]
26. Chaniotis, A.K.; Poulidakos, D. Modeling and optimization of catalytic partial oxidation methane reforming for fuel cells. *J. Power Sources* **2005**, *142*, 184–193. [CrossRef]